Glycobiology, 2023, **33**, 8, 626–636
https://doi.org/10.1093/glycob/cwad051
Advance access publication date 26 June 2023
Original Article

Role of the ST6GAL1 sialyltransferase in regulating ovarian cancer cell metabolism

Robert B. Jones[1], Austin D. Silva[1], Katherine E. Ankenbauer[1], Colleen M. Britain[1], Asmi Chakraborty[1], Jamelle A. Brown[2], Scott W. Ballinger[2,*], Susan L. Bellis[1,*]

[1]Department of Cell, Developmental and Integrative Biology, University of Alabama at Birmingham, Birmingham, AL 35298, United States, [2]Department of Pathology, University of Alabama at Birmingham, Birmingham, AL 35298, United States

*Corresponding author: Department of Cell, Developmental and Integrative Biology, 350A McCallum, University of Alabama at Birmingham, Birmingham, AL 35298, United States. Emails: bellis@uab.edu, scottballinger@uabmc.edu

The ST6GAL1 sialyltransferase, which adds α2–6-linked sialic acids to *N*-glycosylated proteins, is upregulated in many malignancies including ovarian cancer. Through its activity in sialylating select surface receptors, ST6GAL1 modulates intracellular signaling to regulate tumor cell phenotype. ST6GAL1 has previously been shown to act as a survival factor that protects cancer cells from cytotoxic stressors such as hypoxia. In the present study, we investigated a role for ST6GAL1 in tumor cell metabolism. ST6GAL1 was overexpressed (OE) in OV4 ovarian cancer cells, which have low endogenous ST6GAL1, or knocked-down (KD) in ID8 ovarian cancer cells, which have high endogenous ST6GAL1. OV4 and ID8 cells with modulated ST6GAL1 expression were grown under normoxic or hypoxic conditions, and metabolism was assessed using Seahorse technology. Results showed that cells with high ST6GAL1 expression maintained a higher rate of oxidative metabolism than control cells following treatment with the hypoxia mimetic, desferrioxamine (DFO). This enrichment was not due to an increase in mitochondrial number. Glycolytic metabolism was also increased in OV4 and ID8 cells with high ST6GAL1 expression, and these cells displayed greater activity of the glycolytic enzymes, hexokinase and phosphofructokinase. Metabolism maps were generated from the combined Seahorse data, which suggested that ST6GAL1 functions to enhance the overall metabolism of tumor cells. Finally, we determined that OV4 and ID8 cells with high ST6GAL1 expression were more invasive under conditions of hypoxia. Collectively, these results highlight the importance of sialylation in regulating the metabolic phenotype of ovarian cancer cells.

Key words: cancer stem cells; hypoxia; metabolism; sialic acid; ST6GAL1.

Introduction

Aberrant cell surface glycosylation is a well-known characteristic of malignant cells, and certain glycan structures are used clinically as indicators of cancer progression (Munkley and Elliott 2016; Chandler et al. 2019; Rodrigues et al. 2021b; Bellis et al. 2022). However, the functional role of glycoconjugates in driving tumor pathogenesis remains incompletely understood. Tumor-associated changes in glycosylation arise from the dysregulation of a distinct subset of glycosyltransferases and glycosidases. One glycosyltransferase commonly upregulated in cancer is ST6GAL1, a sialyltransferase that adds α2–6-linked sialic acids to *N*-glycosylated proteins bound for the plasma membrane or secretion (Lu and Gu 2015; Bhide and Colley 2017; Garnham et al. 2019; Dorsett et al. 2021). In ovarian cancer, the upregulation of ST6GAL1 is correlated with enhanced metastasis and reduced progression-free and overall patient survival (Schultz et al. 2016; Wichert et al. 2018). The ST6GAL1-mediated addition of α2–6 sialylation to select membrane receptors such as hepatocyte growth factor receptor (HGFR/MET), epidermal growth factor receptor (EGFR/ERBB1), human epidermal growth factor receptor 2 (HER2/ ERBB2), tumor necrosis factor receptor 1 (TNFR1), and β1 integrin modulates the activity of these receptors to induce intracellular signaling cascades that regulate cell phenotype (Seales et al. 2005; Qian et al. 2009; Hou et al. 2016; Duarte et al. 2017; Britain et al. 2018; Holdbrooks et al. 2018; Liu et al. 2018; Rodrigues et al. 2021a; Rao et al. 2022). Our group and others have reported that ST6GAL1 acts as a pro-survival molecule in cancer cells, fostering protection against numerous cytotoxic stressors including inflammatory stimuli, chemotherapy drugs, radiation, and hypoxia (Lee et al. 2010; Park and Lee 2013; Schultz et al. 2013; Chen et al. 2016; Schultz et al. 2016; Chakraborty et al. 2018; Holdbrooks et al. 2018; Jones et al. 2018; Smithson et al. 2022). In particular, we showed that ST6GAL1 activity enhances tumor cell growth under hypoxic conditions by promoting the accumulation and activity of the hypoxia-induced transcription factor, HIF1α (Jones et al. 2018). We also determined that ST6GAL1 imparts a cancer stem cell (CSC) phenotype (Swindall et al. 2013; Schultz et al. 2016). Notably, CSCs are particularly adept at surviving in oxygen-poor conditions, in large part because they modulate their metabolic pathways to sustain cell growth.

One mechanism underlying metabolic adaptation to hypoxia is the upregulation of aerobic glycolysis, a process known as the Warburg effect (Courtnay et al. 2015; Liberti and Locasale 2016; Sancho et al. 2016). Cancer cells commonly use aerobic glycolysis to meet their energy demands (De Francesco et al. 2018). However, evidence has emerged that some cancer cells, especially CSCs, can exhibit metabolic plasticity by activating both glycolysis and oxidative respiration to maintain energy production (Ahmed et al. 2018; Chae and Kim 2018; Jia et al. 2018). Moreover, it has become increasingly apparent that the metabolic phenotype of tumor cells varies from cancer to cancer, and patient to patient. A better understanding of the metabolic processes employed by tumor cells to survive microenvironmental stressors such as hypoxia is needed

Received: March 21, 2022. **Revised:** June 16, 2023. **Accepted:** June 19, 2023

to exploit cellular metabolism as a potential therapeutic vulnerability.

In the current study, we evaluated the role of ST6GAL1 in the metabolism of ovarian cancer cells exposed to either normoxic or hypoxic conditions. To this end, ST6GAL1 was overexpressed in OV4 cells, which have low endogenous ST6GAL1, or knocked-down in ID8 cells, which have robust levels of endogenous ST6GAL1. To induce hypoxia, cells were treated with the hypoxia mimetic desferrioxamine (DFO), and then evaluated for metabolic activity using Seahorse technology and other assays. In the aggregate, our results show that ST6GAL1 activity promotes both oxidative and glycolytic metabolism, as well as increased activation of the key glycolytic enzymes, hexokinase (HK) and phosphofructokinase (PFK). Additionally, cells with high ST6GAL1 expression are more invasive under conditions of hypoxia. This study highlights a new role for ST6GAL1 in the regulation of cancer cell metabolism.

Results

ST6GAL1 activity modulates aerobic metabolism

To investigate the role of ST6GAL1 in cellular metabolism, OV4 ovarian cancer cells were stably transduced with either an empty lentiviral vector (EV) or an ST6GAL1 overexpression (OE) vector (Fig. 1A, see Table 1 for a description of cell models). The enforced expression of ST6GAL1 in OV4 cells led to a concomitant increase in surface α2–6 sialic acids, as measured by staining cells with the SNA lectin, which is specific for α2–6 sialic acids (Fig. 1B). The OV4 line represents one of the few cancer cell lines that lacks detectable endogenous ST6GAL1 protein. Aerobic (mitochondrial) metabolism was quantified by Seahorse technology in OV4 cells exposed to either normoxic or hypoxic conditions. Intracellular hypoxia was chemically induced using the iron chelator, DFO, for 24 h prior to measuring cellular respiration. Figure 1C shows a representative mitochondrial respiration profile for EV and OE cells treated with or without DFO. Mitochondrial respiration profiles were utilized to examine various aspects of mitochondrial energy production. As shown in Fig. 1D, DFO treatment of OV4 EV cells caused a significant drop in the basal mitochondrial respiration rate. In contrast, there was no difference in basal respiration between untreated (UT) OE cells and DFO-treated OE cells. These data indicate that ST6GAL1 OE protects against a DFO-induced reduction in basal respiration. A similar protective effect of ST6GAL1 was observed for the oxygen utilization rate for ATP production, which is the proportion of basal respiration used for ATP generation. DFO treatment significantly decreased the ATP production rate in EV, but not OE, cells (Fig. 1E). Furthermore, ST6GAL1 OE protected against a DFO-dependent loss in the maximal respiration rate (Fig. 1F). We also assessed proton leak (Fig. 1G), but did not observe any significant differences. Proton leakage can be an indicator of mitochondrial health; therefore, it may be inferred that DFO was not overly toxic to the mitochondria. Overall, results in Fig. 1 suggest that ST6GAL1 protects cells from hypoxia-induced decreases in mitochondrial respiration.

Aerobic metabolism was next examined in the ID8 ovarian cancer cell line, which has substantial expression of endogenous ST6GAL1. ID8 cells were transduced with an ST6GAL1-targeting shRNA construct to knock-down (KD) expression

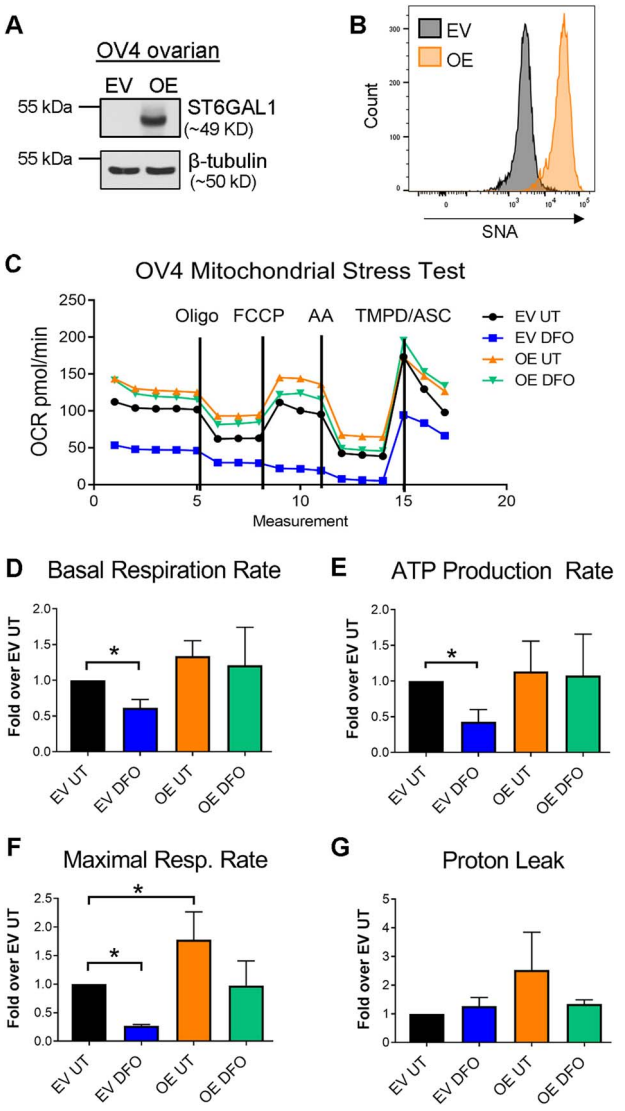

Fig. 1. ST6GAL1 overexpression protects OV4 ovarian cancer cells from a reduction in oxidative metabolism due to hypoxic stress. (A) OV4 cells were stably transduced with a lentivirus encoding ST6GAL1 and overexpression (OE) was confirmed by immunoblotting. Control cells were generated by stable transduction of an empty vector (EV). (B) Increases in cell surface α2–6 sialic acids were confirmed by SNA staining followed by flow cytometry. (C) Representative mitochondrial stress test profile for OV4 cells treated with DFO, or left untreated (UT). (D) Basal respiration rate, (E) ATP production, (F) maximal respiration rate, and (G) proton leak levels for cells treated with or without DFO. Graphs depict means and S.E.M. from three independent experiments. $^*P < 0.05$.

of ST6GAL1 (Fig. 2A). A decrease in surface α2–6 sialylation in KD cells was confirmed by SNA staining (Fig. 2B). Figure 2C depicts a representative mitochondrial respiration profile. Treatment with DFO resulted in decreased basal respiration for both EV and KD cells (Fig. 2D). However, higher levels of basal respiration were maintained in DFO-treated EV cells when compared with DFO-treated KD cells, suggesting that ST6GAL1 provides some degree of protection from hypoxia. ATP production (Fig. 2E) and the maximal respiration rate (Fig. 2F) were also diminished by DFO treatment of EV and KD cells. Trends were noted toward increased ATP production and maximal respiration rate in DFO-treated EV cells relative to DFO-treated KD cells, although these

Table 1. Description of cell models.

Cell Model	Description
OV4 EV	OV4 ovarian cancer cells stably transduced with an empty vector (EV) lentiviral construct. OV4 cells lack expression of endogenous ST6GAL1.
OV4 OE	OV4 ovarian cancer cells stably transduced with an ST6GAL1 overexpression (OE) lentiviral vector.
ID8 EV	ID8 ovarian cancer cells stably transduced with an empty vector (EV) lentivirus. ID8 cells have robust expression of endogenous ST6GAL1.
ID8 KD	ID8 ovarian cancer cells stably transduced with an shRNA-bearing lentiviral vector to knock-down (KD) ST6GAL1.
DFO-treated cells	Cells treated with the hypoxia mimetic, desferrioxamine (DFO).
Untreated (UT) cells	Cells treated with control media lacking DFO.

results were not significant. The values for proton leak were not significantly different between the four groups (Fig. 2G). These results suggest that ST6GAL1 KD reduces mitochondrial respiration primarily by affecting the basal respiration rate.

ST6GAL1 activity does not affect mitochondrial number

To evaluate whether differences in oxidative phosphorylation were associated with alterations in mitochondrial biogenesis, we measured mitochondrial number. To this end, OV4 and ID8 cells were stained with Cytopainter Green, a fluorescent dye that incorporates into the mitochondrial membrane. Representative images for Cytopainter Green stained OV4 and ID8 cells are depicted in Fig. 3A. Relative mitochondrial number was quantified in cells treated with or without DFO by measuring mean fluorescence. As shown in Fig. 3B, treatment of OV4 EV and OE cells with DFO increased the mean fluorescence when compared with their respective untreated controls. However, no significant differences were observed between DFO-treated EV and DFO-treated OE cells. Similarly, DFO treatment increased fluorescence in ID8 EV and KD cells, but no significant differences were noted in DFO-treated KD cells relative to DFO-treated EV cells (Fig. 3C). Thus, the effects of ST6GAL1 on mitochondrial respiration were not due to an alteration in mitochondrial number. Finally, to exclude the possibility that any variations in mitochondrial respiration were associated with DFO-induced cytotoxicity, we performed a Caspase Glo apoptosis assay. No significant differences in caspase activity subsequent to DFO treatment were detected in OV4 or ID8 cells (Fig. 3D and E, respectively).

ST6GAL1 activity enhances glycolytic metabolism

The role of ST6GAL1 in regulating glycolytic metabolism was next assessed by performing glycolytic stress tests on cells treated with or without DFO. Figure 4A shows a representative profile in the OV4 cell line. Quantification of the rate of glycolysis, glycolytic capacity, and glycolytic reserve revealed no significant differences between untreated EV and untreated OE cells (Fig. 4B–D, respectively). Furthermore, DFO treatment did not appear to significantly alter any of these parameters. However, DFO-treated OE cells displayed significantly higher rates of glycolysis and glycolytic capacity (Fig. 4B,C), but not glycolytic reserve (Fig. 4D), when compared with DFO-treated EV cells. These data suggest that ST6GAL1 activity facilitates glycolytic metabolism under conditions of hypoxia. The non-glycolytic acidification rate (NGAR), a measure of extracellular acidification not attributable to glycolysis, was also examined. Significantly higher rates of non-glycolytic acidification were detected in DFO-treated EV and OE cells compared with untreated EV and OE cells (Fig. 4E). Additionally, the non-glycolytic acidification rate was significantly higher in DFO-treated OE cells versus DFO-treated EV cells. The NGAR can be attributed to metabolic processes such as glycogenolysis and the TCA cycle, indicating that other aspects of cancer cell metabolism might be regulated by ST6GAL1, although this will require further investigation.

Glycolytic stress tests were subsequently conducted for ID8 cells. A representative metabolic profile is shown in Fig. 5A. As with OV4 cells, DFO treatment of EV and KD cells did not alter the glycolytic rate or glycolytic capacity (Fig. 5B,C), although glycolytic reserve (Fig. 5D) was decreased in DFO-treated EV cells when compared with untreated EV cells. Notably, untreated EV cells exhibited higher levels of glycolysis and glycolytic capacity than untreated KD cells (Fig. 5B,C). Untreated EV cells also had an enrichment in the non-glycolytic acidification rate relative to untreated KD cells (Fig. 5E). These data suggest that ST6GAL1 activity enhances glycolytic metabolism in ID8 cells under conditions of normoxia.

ST6GAL1 increases the overall metabolism of ovarian cancer cells

Metabolism maps were generated from the aerobic and glycolytic metabolic data to obtain a broader view of the overall metabolic state of the cells. As shown in Fig. 6A, untreated OV4 OE cells were more energetic in both their glycolytic and aerobic metabolism when compared to the more quiescent, untreated OV4 EV cells. Upon treatment with DFO, EV cells increased their glycolytic metabolism, whereas DFO-treated OE cells exhibited an enrichment in both glycolytic and aerobic metabolism. An energy map was also created for the ID8 cell line (Fig. 6B). Untreated ID8 EV cells had higher rates of glycolytic and oxidative metabolism than untreated ID8 KD cells. Thus, in both the OV4 and ID8 cell models, ST6GAL1 activity enhanced the overall metabolic activity of cells under conditions of normoxia. When treated with DFO, ID8 EV and KD cells decreased their oxidative metabolism; however, glycolytic metabolism was increased in both cell lines. Importantly, DFO-treated ID8 EV cells maintained much higher levels of aerobic metabolism than DFO-treated KD cells. Together, results from the OV4 and ID8 cell models suggest that ST6GAL1 contributes to a more active metabolic state.

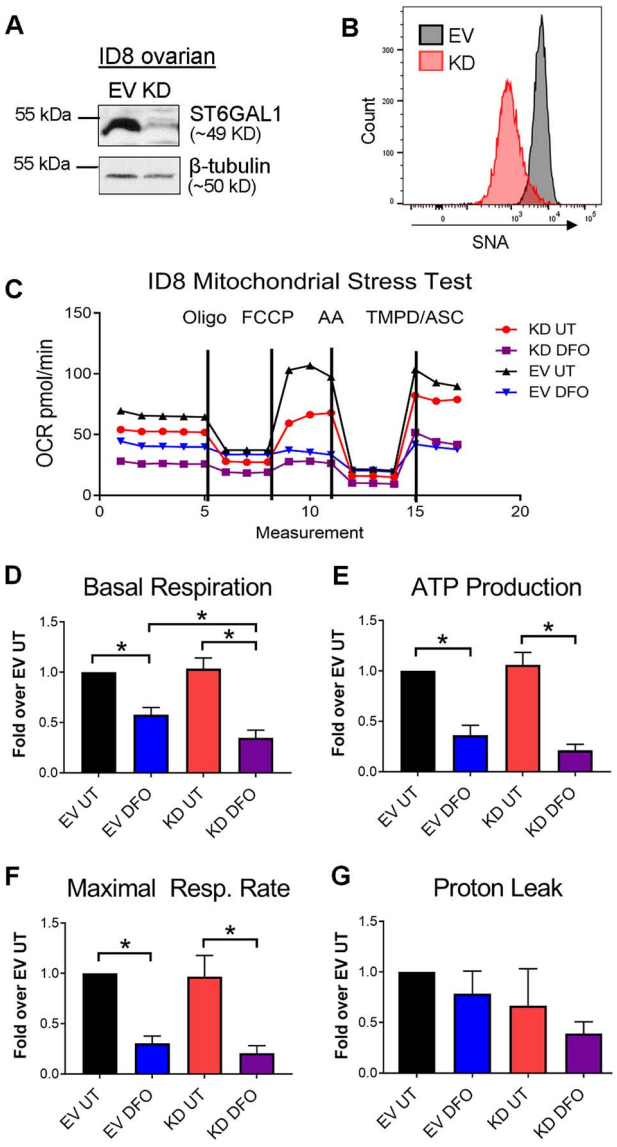

Fig. 2. ST6GAL1 activity enhances basal respiration in hypoxic ID8 cells. ID8 cells were stably transduced with ST6GAL1 targeting shRNA, and ST6GAL1 knockdown (KD) was confirmed by immunoblotting. Control ID8 cells were generated by stable transduction of an empty vector (EV). (B) A decrease in surface α2–6 sialylation was confirmed by SNA staining. (C) Representative mitochondrial stress test for ID8 cell models treated with or without DFO. (D) Basal respiration rate, (E) ATP production, (F) maximal respiration rate, and (G) proton leak levels for cells treated with or without DFO. Graphs depict mean and S.E.M. from three independent experiments. $^*P < 0.05$.

ST6GAL1 increases the activity of glycolytic enzymes

To assess potential mechanisms by which ST6GAL1 enhances the glycolytic metabolism of OV4 and ID8 cells, we examined the activity of two rate limiting enzymes in glycolysis, HK and PFK. In OV4 cells, significantly higher HK activity was noted in OE compared with EV cells under normoxic conditions (Fig. 7A). However HK activity was comparable in the hypoxic EV and OE cells (Fig. 7A), which is interesting in view of the fact that glycolytic metabolism is increased in DFO-treated OE vs. DFO-treated EV cells (Fig. 6A). Thus, changes in enzymes other than HK likely underlie ST6GAL1's contribution to glycolytic metabolism under hypoxic conditions. Importantly, PFK activity was significantly increased in OE cells under both normoxic and hypoxic conditions when compared with EV cells (Fig. 7A). It is possible that PFK, and/or other metabolic enzymes not evaluated in the current study, represent the major mediators of ST6GAL1's effects on glycolysis in hypoxic cells. Relevant to this concept, Tanner et al. reported that PFK was a more potent activator of glycolytic flux than HK (Tanner et al. 2018). In the ID8 cell model, KD of ST6GAL1 expression suppressed the activity of HK in normoxia, and PFK in hypoxia. (Fig. 7B). Hence, PFK is consistently activated in OV4 and ID8 cells with high ST6GAL1 expression under conditions of low oxygen tension.

ST6GAL1 activity promotes cell invasion under conditions of hypoxia

It is well-known that hypoxic conditions can induce cells to become more invasive (Shi et al. 2021; Parlani et al. 2023). We therefore examined invasiveness in OV4 and ID8 cells using 3D invasion assays. As shown in Fig. 8A, OV4 OE cells were more invasive than EV cells at 48 h after DFO treatment. Similarly, ID8 EV cells were more invasive than KD cells at 48 h after DFO treatment (Fig. 8B). These data suggest that ST6GAL1 activity promotes the invasiveness of cells exposed to hypoxia.

Discussion

An alteration in cellular metabolism was one of the earliest known hallmarks of a cancer cell (Warburg 1925; Warburg et al. 1927). Neoplastic changes in metabolism contribute to a tumor cell's proliferative capability, as well as acquisition of chemoresistance (Hanahan and Weinberg 2011; Rahman and Hasan 2015). Therapeutic targeting of cancer cell metabolism is a promising area of investigation because it may offer a path to harm cancer cells without significantly disrupting normal cell function (Snyder et al. 2018). However, one obstacle hindering the development of metabolic interventions is the ability of malignant cells to modulate their metabolic phenotype in response to distinct tumor microenvironments (Jia et al. 2018; Thongon et al. 2018). Cancer cells are very adept at switching to alternative sources of energy when one energy source becomes compromised. How this metabolic plasticity is regulated is currently an intensive area of research.

In the present study, we examined the role of ST6GAL1-mediated sialylation in the regulation of cancer cell metabolism. We determined that enforced expression of ST6GAL1 in OV4 ovarian cancer cells enabled cells to maintain high levels of mitochondrial respiration in the presence of the hypoxia mimetic DFO. This activity is expected to impart a survival advantage, as cancer cells would be able to sustain their proliferative potential within the hypoxic tumor milieu. ST6GAL1 KD in ID8 cells led to impaired basal respiration under conditions of DFO-induced hypoxia, however the overall effects of ST6GAL1 on mitochondrial metabolism in the ID8 model were less pronounced than those observed in OV4 cells. In addition to mitochondrial respiration, ST6GAL1 activity facilitated glycolytic metabolism in both the OV4 and ID8 cell models. In ID8 cells, ST6GAL1 KD reduced the capability of cells to perform glycolysis under normoxic conditions, whereas in OV4 cells, ST6GAL1 OE promoted glycolytic activity

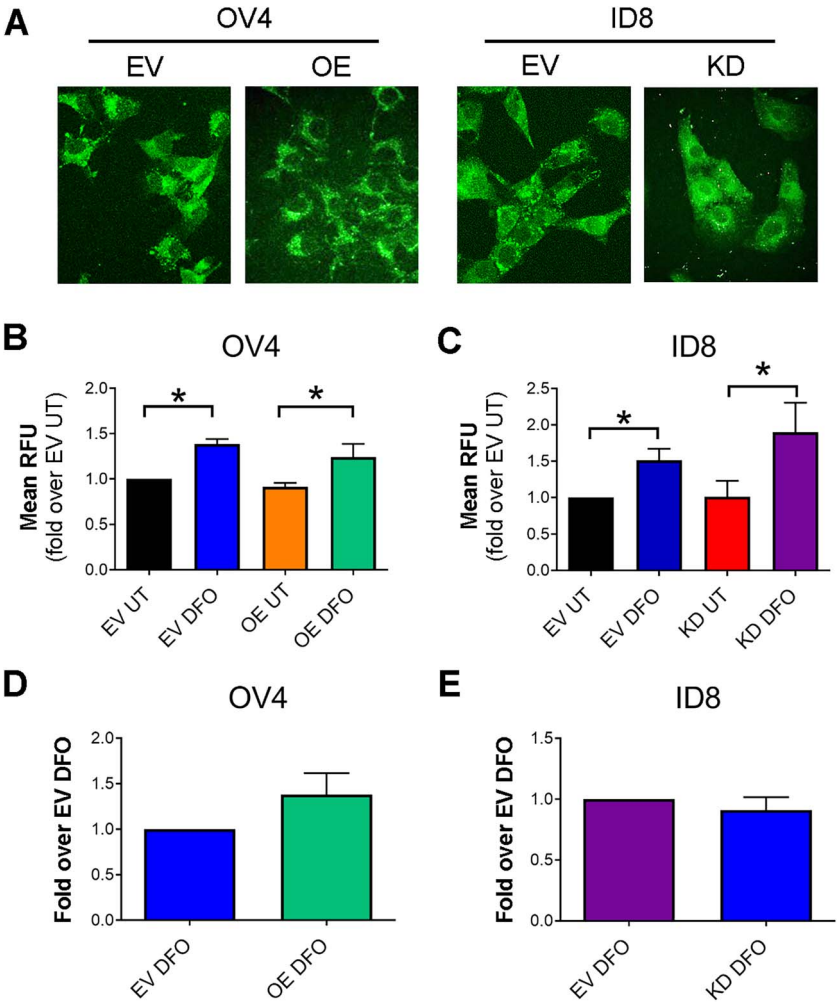

Fig. 3. ST6GAL1 activity does not alter mitochondrial number. Representative images of OV4 and ID8 cells stained with the Cytopainter Green mitochondrial dye. (B–C) Mean fluorescent intensity of OV4 (B) or ID8 (C) cells treated with or without DFO and then stained with Cytopainter Green. (D–E) caspase Glo apoptosis assays conducted on OV4 (D) and ID8 (E) cells treated with DFO. Graphs depict mean and S.E.M. from at three independent experiments. $^{*}P < 0.05$.

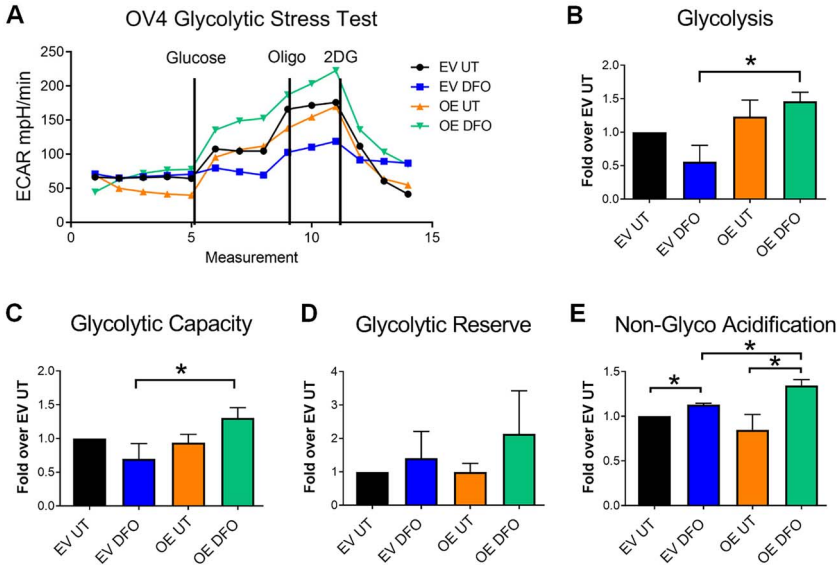

Fig. 4. ST6GAL1 activity contributes to increased glycolytic metabolism in hypoxic OV4 cells. Representative glycolytic stress test profile in OV4 cells treated with and without DFO. (B) Glycolytic rate, (C) glycolytic capacity, (D) glycolytic reserve, and (E) non-glycolytic acidification rate of cells treated with and without DFO. Graphs depict mean and S.E.M. from three independent experiments. $^{*}P < 0.05$.

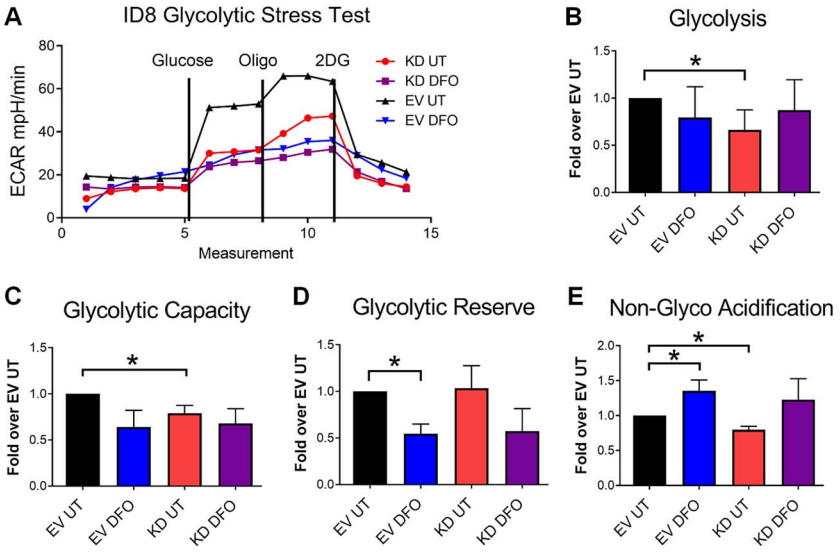

Fig. 5. ST6GAL1 activity contributes to increased glycolytic metabolism in ID8 cells under normoxia. Representative glycolytic stress test profile for ID8 cells treated with and without DFO. (B) Glycolytic rate, (C) glycolytic capacity, (D) glycolytic reserve, and (E) non-glycolytic acidification rate of cells treated with and without DFO. Graphs depict mean and S.E.M. from three independent experiments. $^*P < 0.05$.

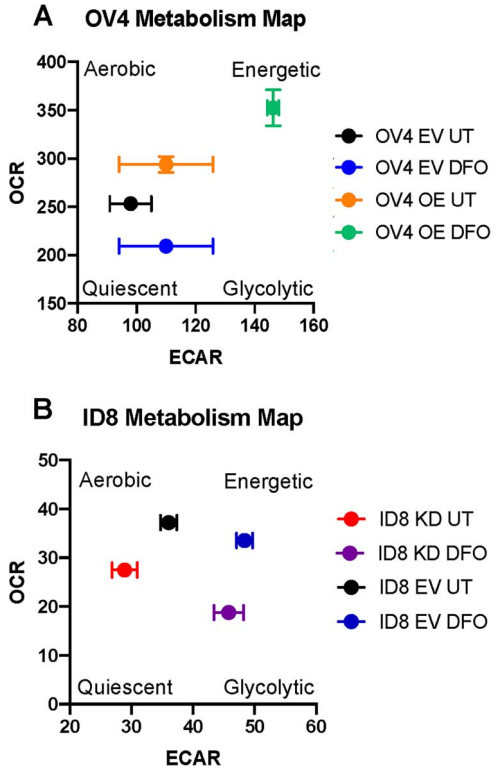

Fig. 6. Metabolic maps of OV4 and ID8 cells. Representative metabolic maps of OV4 (A) and ID8 (B) cells treated with or without DFO.

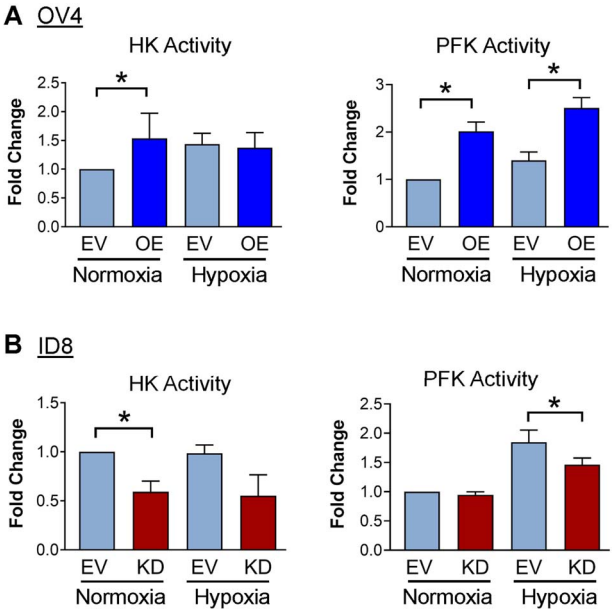

Fig. 7. ST6GAL1 promotes increased activity of key glycolytic enzymes. OV4 (A) and ID8 (B) cells were cultured under normoxic conditions, or in a hypoxia chamber (0.5 percent O_2) for 48 h. The activity of hexokinase (HK) and phosphofructokinase (PFK) was subsequently quantified. Graphs depict mean and S.E.M. from at least three independent experiments. $^*P < 0.05$.

when the cells were stressed by the hypoxia mimetic DFO. In line with elevated glycolytic metabolism, OV4 and ID8 cells with high ST6GAL1 expression had increased activity of the glycolytic enzymes, HK and PFK. This correspondence between enriched glycolytic rate and increased HK and PFK activity was mirrored by metabolic maps generated from Seahorse data, which implicated a positive role for ST6GAL1 in stimulating metabolism. Together, these findings suggest that ST6GAL1 modulates tumor cell metabolism to sustain energy production.

In both OV4 and ID8 cancer cells, ST6GAL1 activity appeared to promote a more metabolically active phenotype, although some cell type-specific differences were noted in ST6GAL1's contribution to mitochondrial and glycolytic respiration, as well as cellular response to DFO. Given these differences, we speculate that the effects of ST6GAL1 on metabolism may be secondary to ST6GAL1's known role in conferring CSC characteristics (Schultz et al. 2016), rather than through direct regulation of a specific metabolic pathway. Although we have not evaluated CSC characteristics in the OV4 and ID8 cell models, we previously reported

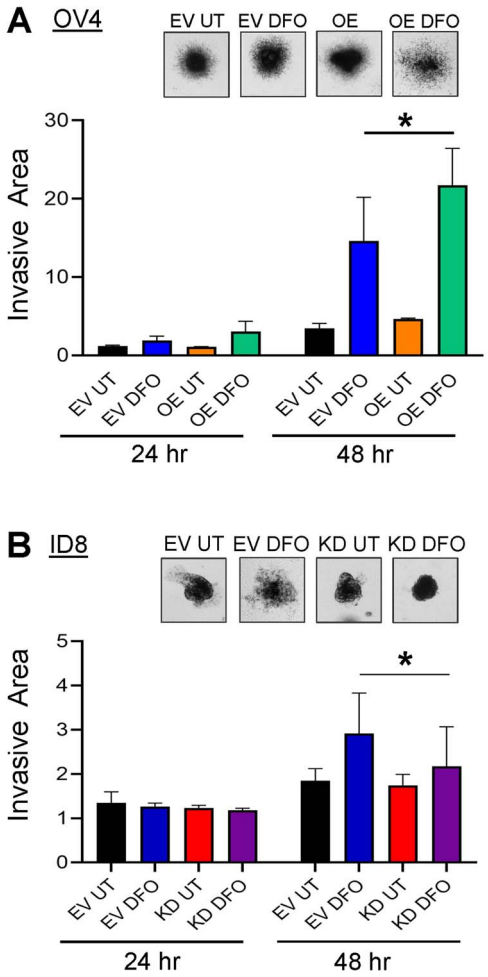

Fig. 8. ST6GAL1 enhances the invasiveness of hypoxic cells. OV4 (A) and ID8 (B) cells were treated with or without DFO and then evaluated for invasion using a 3D spheroid invasion assay. The formation of invadopodia was quantified by Image J. Graphs depict mean and S.E.M. from three independent experiments. $^{*}P < 0.05$.

that ST6GAL1 imparts CSC properties in multiple ovarian, pancreatic, and colon cancer cell lines, as well as in primary tumor cells from ovarian cancer patients (Swindall et al. 2013; Schultz et al. 2016). On the other hand, the finding that ST6GAL1 regulates metabolism through somewhat different mechanisms in diverse cell models is not inconsistent with the literature, as the metabolic phenotype of cancer cells is known to vary depending upon factors such as cancer type, model system, and experimental design (Sancho et al. 2016; Peixoto and Lima 2018). Even within a specific cancer, such as ovarian cancer, the metabolic phenotype may be cell model dependent, as both glycolytic and oxidative metabolic phenotypes have been described (Anderson et al. 2014; Pasto et al. 2014). Although it was previously thought that cancer cells upregulate glycolysis at the expense of oxidative phosphorylation, recent studies have indicated that some cancer cells upregulate both oxidative phosphorylation and glycolysis, and can even switch between these pathways depending upon the tumor milieu (DeBerardinis and Chandel 2016). This metabolic plasticity is particularly characteristic of CSCs, and functions to enable maintenance of proliferative capability in response to whatever tumor microenvironment CSCs find themselves in (De Francesco et al. 2018).

Interestingly, emerging evidence suggests that metabolic alterations may play a broader role in regulating tumor cell phenotype. It is now suggested that altered metabolism can, in and of itself, impart stem-like characteristics (Menendez and Alarcon 2014; De Francesco et al. 2018). This "metabostemness" hypothesis posits that metabolic pathways modulate stemness through the regulation of epigenetic and transcriptional networks. Furthermore, certain metabotypes appear to directly impel differentiated cancer cells to adopt features of CSCs. One question that should be addressed in future studies is whether ST6GAL1's activity in altering cell metabolism is related to a more general reprogramming of cancer cells into a CSC phenotype.

The specific sialylated receptors that mediate enhanced metabolic activity in cells with high ST6GAL1 expression remain to be determined. However, it is noteworthy that ST6GAL1 sialylates, and thereby activates, various receptor tyrosine kinases (RTKs) including EGFR, ERBB2, MET and PDGFRB (Aasheim et al. 1993; Qian et al. 2009; Duarte et al. 2017; Liu et al. 2018; Britain et al. 2021; Gc et al. 2022; Rao et al. 2022). RTKs play prominent roles in cellular metabolism, in part, through the activation of the PI3K/AKT signaling cascade. For instance, signaling by the EGFR/PI3K/AKT node induces expression of select glucose transporters, and this pathway also activates mTORC1, a major metabolic regulator (Orofiamma et al. 2022). Furthermore, EGFR contributes to the ability of cells to adapt to hypoxia, as EGFR/AKT signaling leads to increased translation of HIF1α (Semenza 2003). On the other hand, signaling by the TNFR1/NFκB pathway promotes the transcription of HIF1α, and NFκB binds directly to the HIF1α promoter (Jung et al. 2003; Gorlach and Bonello 2008; van Uden et al. 2008). It has been previously shown that ST6GAL1-mediated sialylation of TNFR1 stimulates NFκB activation (Holdbrooks et al. 2018), and NFκB is also one of the main pathways that drives CSC characteristics (Rinkenbaugh and Baldwin 2016).

While additional studies will be needed to understand ST6GAL1's mechanism of action, results from the present investigation point to a novel role for ST6GAL1 in sustaining the metabolism of ovarian cancer cells. The clinical targeting of metabolic pathways to suppress tumor cell growth is a highly active area of research; however, limited attention has been paid to interventions directed at glycosylation-dependent pathways. Given its many pro-tumorigenic functions, ST6GAL1 is an attractive therapeutic target. Sialyltransferase inhibitors, including artificial sialic acid analogues, have proven effective in suppressing tumor growth (Bull et al. 2018); however, many of these agents broadly target the sialyltransferase family and consequently have off-target effects. More specific inhibitors for ST6GAL1 are currently being developed by the Skropeta laboratory (Dobie et al. 2021). As an alternative to sialyltransferase inhibitors, the Bertozzi group generated a bivalent antibody engineered with a Her2-binding sequence and an active sialidase enzyme (Xiao et al. 2016). The Her2-binding domain directs antibody binding to breast cancer cells, and then the sialidase cleaves sialic acids from the tumor cell surface. This approach enables the de-sialylation of tumor cells without impacting other cell types. These emerging strategies for selective targeting of abnormal tumor cell sialylation, such as elevated α2,6 sialylation, hold great promise for the development of alternative cancer treatments. The finding that ST6GAL1

helps to sustain the metabolic activity of ovarian cancer cells not only highlights a new function for ST6GAL1 but also points to a novel avenue for modulating the metabolic activity of tumor cells.

Materials and methods

Cell culture

ID8 murine ovarian cancer cells were provided by Dr. Carrie Rinker-Schaeffer (University of Chicago) and OV4 human ovarian cancer cells were a gift from Dr. Timothy Eberlein (Harvard University). As in our prior publications (Schultz et al. 2013; Britain et al. 2018), OV4 cells were stably transduced with lentivirus harboring the ST6GAL1 overexpression vector, whereas ID8 cells were stably transduced with lentivirus containing an ST6GAL1 knockdown vector. Polyclonal cell populations were isolated via puromycin selection. For routine propagation, ID8 cells were grown in Dulbecco's modified Eagle's medium (DMEM), whereas OV4 cells were grown in Dulbecco's modified Eagle's medium/F12 (DME/F12). Both of these media were supplemented with 10 percent (v/v) fetal bovine serum (FBS) (Atlanta Biologicals) and 1 percent (v/v) antibiotics/antimycotics (GE Healthcare/Hyclone). For hypoxia mimetic studies, cells were grown in media with 1 percent FBS and DFO (Sigma) added at a final concentration of 150 μM (Peyssonnaux et al. 2007). For physiological hypoxia studies, cells were cultured in 1 percent FBS media in a hypoxia chamber containing 0.5 percent O_2. Changes in ST6GAL1 expression were confirmed via immunoblotting with a goat polyclonal ST6GAL1 antibody (R&D Systems AF5924). To verify changes in cell surface α2–6 sialic acid, cells were stained with Cy5-tagged *Sambucus nigra agglutinin* (SNA) (Vector Labs), and evaluated by flow cytometry on an LSR Fortessa (BD Biosciences). Data were analyzed using FlowJo software.

Seahorse XFe96 quantification of cellular metabolism

In sum, 10,000 cells were plated in each well of a 96 well Seahorse tissue culture plate and allowed to attach overnight. Cells were then treated in the appropriate media with or without DFO for 24 hs. After cell treatment with or without DFO, aerobic (mitochondrial) metabolism was assayed after removal of media and addition of 180 μL of XF assay media pH 7.4 (Agilent) supplemented with 25-mM glucose and 200-mM L-glutamine. To ensure excess CO_2 was removed from the assay media, the plate was placed in a CO_2 free incubator for 1 h prior to the start of the assay. Effectors at a 10X concentration were then loaded into the injector ports of the cartridge. To obtain the mitochondrial stress profile, a baseline was established for five cycles (each cycle consisted of a 3-min mixing time, 2-min wait, and 3-min measuring period). Following this interval, 20 μL of 60 μg/ml of oligomycin were injected into the well to obtain a final concentration of 6 μg/ml. The cellular response was measured for three cycles. Next, 20 μL of 10-μM FCCP were injected into the wells to obtain a final concentration of 1 μM. Cellular response was measured for three cycles. Finally, 20 μL of 100-μM antimycin A were injected into the wells to obtain a final concentration of 10 μM. Cellular response was measured for three cycles. To assess glycolytic metabolism via cellular acidification rates, cells were treated overnight with or without DFO, and culture media was replaced with 180 μL of XF assay media pH 7.4 supplemented with 2-mM L-glutamine. After a baseline was established, 20 μL of 100-mM glucose were injected into the wells to achieve a final concentration of 10 mM, and cellular response was measured for three cycles, followed by oligomycin injection and measured as described above. Finally, 1 M 2-deoxyglucose (2DG) were injected into the wells, to a final concentration of 100-mM 2DG, and cellular response was measured for three cycles. After completion of all assays, cells were fixed with 3.7 percent paraformaldehyde (PFA) for 1 h and stained with 0.5 percent (w/v) crystal violet solution for 1 h. A 10 percent acetic acid solution was then used to solubilize crystal violet-stained cells, and the absorbance of the solution was determined on a Biotek Synergy H1 plate reader at 590 nm. Absorbance values were used as an indirect measure of cell number, and data were normalized to these values. At least three independent experiments were performed and differences I aerobic and glycolytic metabolic profiles were determined using a Student's *t* test.

Calculation of aerobic and glycolytic measures

Calculations for aerobic and glycolytic profiles were performed following the Agilent technologies protocols for mitochondrial stress test and glycolytic stress test (Agilent Technologies User Guides for: XF Cell Mito Stress Test and XF Glycolysis Stress Test). These values were then normalized to EV untreated control cells. At least three independent experiments were performed and differences in aerobic and glycolytic metabolism profiles were calculated using a Student's *t* test.

Hexokinase and phosphofructokinase assays

Cells were cultured in either 0.5 percent oxygen, or normoxic conditions, for 48 h in media containing 1 percent FBS. Duplicate wells were plated so that results could be normalized to cell number. After incubation in normoxia or hypoxia, cells were evaluated for HK and PFK activity using kits from Abcam (catalog # ab136957 and ab155898, respectively). Enzyme assays were conducted in accordance with protocols provided by the manufacturer. Absorbance values, reflecting enzyme activity, were measured using a Biotek plate reader. To quantify the cell number, cells in the duplicate wells were fixed with 3.7 percent PFA, stained with crystal violet, and solubilized in 10 percent acetic acid as before. Absorbance values from crystal violet-stained cultures were used to normalize enzyme activity to the relative cell number. At least three independent experiments were performed and differences in enzymatic activity were determined using a Student's *t* test.

Measurement of mitochondrial number

In sum, 40,000 cells were seeded onto coverslips pre-treated with poly-D-lysine and allowed to attach overnight. The growth media was then replaced with treatment media with or without 150 μM DFO. After a 24-h incubation, cells were stained with the fluorescent mitochondrial dye, Cytopainter Green (Abcam, catalog# ab176830) following the manufacturer's protocol. Briefly, cells were stained with Cytopainter Green for 2 h, and then washed with phosphate-buffered saline (PBS) to remove excess dye. Coverslips were mounted on slides using Prolong Gold mounting media (Thermo Fisher). Representative images were obtained using a Nikon A1R confocal microscope. For a quantitative

determination of mitochondria number, 10,000 cells were plated in a clear bottom, black-sided, 96 well plate, and allowed to attach overnight. Quadruplicate wells were set up; two for measuring mitochondria number, and two for quantifying total cell number. Cells were treated for 24 h with media containing or lacking 150-μM DFO. Following this incubation, two of the wells were stained with Cytopainter Green, and the mean fluorescence of the samples was measured using a Biotek plate reader at Ex/Em of 498/520 nm. The other two wells were stained with crystal violet, solubilized with acetic acid, and absorbance values were measured on a Biotek plate reader. Values from crystal violet-stained cultures were used to normalize the mean fluorescence of Cytopainter Green-stained cultures to relative cell number. At least three independent experiments were performed, and differences in mitochondrial number were determined using a Student's *t* test.

Apoptosis assays

Cells were seeded at a density of 40,000 cells/well into 12-well plates and allowed to attach overnight. Cells were then treated in duplicate with DFO for 24 h. One plate was used for a Caspase Glo apoptosis assay (Promega) by adding 300 uL per well of the Caspase Glo reagent, and incubating cells for 30 min at room temperature. Samples were loaded into a 96 well-plate in triplicate, and luminescence values were measured using a BioTek plate reader. To normalize for cell number, the second plate was stained with crystal violet, solubilized with acetic acid and absorbance values measured as before. At least three independent experiments were performed and differences in caspase activity were determined using a Student's *t* test.

3D spheroid invasion assay

Tumor cell invasion was assessed using a 3D spheroid invasion assay as previously described (Berens et al. 2015). Cells were treated with or without 150-μM DFO in 1 percent FBS for 24 h, and then cells were grown in hanging drop suspensions for 72 h. Spheroids formed in suspension were resuspended in Matrigel and grown in media with 10 percent FBS. Images of spheroids and invadopodia were captured using a bright-field microscope at 24 and 48 h. Invasion into the matrix was quantified using ImageJ software. Results shown are from three independent experiments, and significance was evaluated using a Student's *t* test.

Abbreviations

CSC, cancer stem cells; DFO, desferrioxamine; ECAR, extracellular acidification rate; EGFR, epidermal growth factor receptor; ERBB2, Erb-B2 receptor tyrosine kinase 2; HK, hexokinase; MET, mesenchymal epithelial transition factor receptor (a.k.a. HGF receptor); NGAR, non-glycolytic acidification rate; OCR, oxygen consumption rate; PFK, phosphofructokinase; ST6GAL1, β-galactoside α2,6 sialyltransferase 1; TNFR1, tumor necrosis factor receptor 1

Authors' contributions

Robert B. Jones (Conceptualization-Lead, Data curation-Lead, Formal analysis-Equal, Methodology-Equal, Writing—original draft-Lead, Writing—review and editing-Equal), Austin Silva (Conceptualization-Equal, Data curation-Equal, Formal analysis-Equal, Methodology-Equal, Writing—review and editing-Equal), Katherine Ankenbauer (Conceptualization-Equal, Data curation-Equal, Formal analysis-Equal, Methodology-Equal, Writing—review and editing-Equal), Colleen M. Britain (Data curation-Equal, Formal analysis-Equal, Writing—original draft-Supporting), Asmi Chakraborty (Data curation-Equal, Formal analysis-Equal, Writing—original draft-Supporting), Jamelle A. Brown (Data curation-Equal, Formal analysis-Equal, Methodology-Equal, Writing—original draft-Supporting, Writing—review and editing-Supporting), Scott W. Ballinger (Conceptualization-Equal, Data curation-Equal, Formal analysis-Equal, Funding acquisition-Equal, Methodology-Equal, Project administration-Equal, Resources-Equal, Supervision-Equal, Writing—original draft-Equal, Writing—review and editing-Equal), Susan Bellis (Conceptualization-Equal, Data curation-Equal, Formal analysis-Equal, Funding acquisition-Equal, Methodology-Equal, Project administration-Equal, Resources-Equal, Supervision-Equal, Writing—original draft-Equal, Writing—review and editing-Equal).

Funding

This work was supported by the National Institutes of Health (CA225177 and CA233581 to S.L.B., HL103859 to S.W.B.). R.B.J., C.M.B., K.E.A., and A.D.S. were supported by Predoctoral Fellowships funded by the National Institutes of Health T32 Training Program in Cell, Molecular and Developmental Biology (GM008111). J.A.B. was supported by the A.G. Minnie Gaston Predoctoral Fellowship.

Conflict of interest statement. None declared.

Data availability statement

All data generated or analyzed during this study are included in this paper.

References

Aasheim HC, Aas-Eng DA, Deggerdal A, Blomhoff HK, Funderud S, Smeland EB. Cell-specific expression of human beta-galactoside alpha 2,6-sialyltransferase transcripts differing in the 5′ untranslated region. *Eur J Biochem*. 1993:**213**(1):467–475.

Ahmed N, Escalona R, Leung D, Chan E, Kannourakis G. Tumour microenvironment and metabolic plasticity in cancer and cancer stem cells: perspectives on metabolic and immune regulatory signatures in chemoresistant ovarian cancer stem cells. *Semin Cancer Biol*. 2018:**53**:265–281.

Anderson AS, Roberts PC, Frisard MI, Hulver MW, Schmelz EM. Ovarian tumor-initiating cells display a flexible metabolism. *Exp Cell Res*. 2014:**328**(1):44–57.

Bellis SL, Reis CA, Varki A, Kannagi R, Stanley P. Glycosylation changes in cancer. In: Varki A, Cummings RD, Esko JD, Stanley P, Hart GW, Aebi M, Kinoshita T, Mohnen D, Packer NH, Prestegard JH, et al., editors. *Essentials of glycobiology, Chapter 47*. Cold Spring Harbor, NY: Cold Spring Harbor Laboratory Press; 2022. pp. 631–644

Berens EB, Holy JM, Riegel AT, Wellstein A. A cancer cell spheroid assay to assess invasion in a 3D setting. *J Vis Exp*. 2015:**105**(105):53409.

Bhide GP, Colley KJ. Sialylation of N-glycans: mechanism, cellular compartmentalization and function. *Histochem Cell Biol*. 2017:**147**(2):149–174.

Britain CM, Bhalerao N, Silva AD, Chakraborty A, Buchsbaum DJ, Crowley MR, et al. Glycosyltransferase ST6Gal-I promotes the epithelial to mesenchymal transition in pancreatic cancer cells. *J Biol Chem*. 2021:**296**:100034.

Britain CM, Holdbrooks AT, Anderson JC, Willey CD, Bellis SL. Sialylation of EGFR by the ST6Gal-I sialyltransferase promotes EGFR activation and resistance to gefitinib-mediated cell death. *J Ovarian Res*. 2018:**11**(1):12.

Bull C, Boltje TJ, Balneger N, Weischer SM, Wassink M, van Gemst JJ, et al. Sialic acid blockade suppresses tumor growth by enhancing T-cell-mediated tumor immunity. *Cancer Res*. 2018:**78**(13): 3574–3588.

Chae YC, Kim JH. Cancer stem cell metabolism: target for cancer therapy. *BMB Rep*. 2018:**51**(7):319–326.

Chakraborty A, Dorsett KA, Trummell HQ, Yang ES, Oliver PG, Bonner JA, et al. ST6Gal-I sialyltransferase promotes chemoresistance in pancreatic ductal adenocarcinoma by abrogating gemcitabine-mediated DNA damage. *J Biol Chem*. 2018:**293**(3): 984–994.

Chandler KB, Costello CE, Rahimi N. Glycosylation in the tumor microenvironment: implications for tumor angiogenesis and metastasis. *Cell*. 2019:**8**(6):53.

Chen X, Wang L, Zhao Y, Yuan S, Wu Q, Zhu X, et al. ST6Gal-I modulates docetaxel sensitivity in human hepatocarcinoma cells via the p38 MAPK/caspase pathway. *Oncotarget*. 2016:**7**(32): 51955–51964.

Courtnay R, Ngo DC, Malik N, Ververis K, Tortorella SM, Karagiannis TC. Cancer metabolism and the Warburg effect: the role of HIF-1 and PI3K. *Mol Biol Rep*. 2015:**42**(4):841–851.

De Francesco EM, Sotgia F, Lisanti MP. Cancer stem cells (CSCs): metabolic strategies for their identification and eradication. *Biochem J*. 2018:**475**(9):1611–1634.

DeBerardinis RJ, Chandel NS. Fundamentals of cancer metabolism. *Sci Adv*. 2016:**2**(5):e1600200.

Dobie C, Montgomery AP, Szabo R, Yu H, Skropeta D. Synthesis and biological evaluation of selective phosphonate-bearing 1,2,3-triazole-linked sialyltransferase inhibitors. *RSC Med Chem*. 2021:**12**(10):1680–1689.

Dorsett KA, Marciel MP, Hwang J, Ankenbauer KE, Bhalerao N, Bellis SL. Regulation of ST6GAL1 sialyltransferase expression in cancer cells. *Glycobiology*. 2021:**31**(5):530–539.

Duarte HO, Balmana M, Mereiter S, Osorio H, Gomes J, Reis CA. Gastric cancer cell glycosylation as a modulator of the ErbB2 oncogenic receptor. *Int J Mol Sci*. 2017:**18**(11):2262.

Garnham R, Scott E, Livermore KE, Munkley J. ST6GAL1: a key player in cancer. *Oncol Lett*. 2019:**18**(2):983–989.

Gc S, Tuy K, Rickenbacker L, Jones R, Chakraborty A, Miller CR, et al. alpha2,6 sialylation mediated by ST6GAL1 promotes glioblastoma growth. *JCI Insight*. 2022:**7**(21):e158799.

Gorlach A, Bonello S. The cross-talk between NF-kappaB and HIF-1: further evidence for a significant liaison. *Biochem J*. 2008:**412**(3):e17–e19.

Hanahan D, Weinberg RA. Hallmarks of cancer: the next generation. *Cell*. 2011:**144**(5):646–674.

Holdbrooks AT, Britain CM, Bellis SL. ST6Gal-I sialyltransferase promotes tumor necrosis factor (TNF)-mediated cancer cell survival via sialylation of the TNF receptor 1 (TNFR1) death receptor. *J Biol Chem*. 2018:**293**(5):1610–1622.

Hou S, Hang Q, Isaji T, Lu J, Fukuda T, Gu J. Importance of membrane-proximal N-glycosylation on integrin beta1 in its activation and complex formation. *FASEB J*. 2016:**30**(12):4120–4131.

Jia D, Park JH, Jung KH, Levine H, Kaipparettu BA. Elucidating the metabolic plasticity of cancer: mitochondrial reprogramming and hybrid metabolic states. *Cell*. 2018:**7**(3):21.

Jones RB, Dorsett KA, Hjelmeland AB, Bellis SL. The ST6Gal-I sialyltransferase protects tumor cells against hypoxia by enhancing HIF-1alpha signaling. *J Biol Chem*. 2018:**293**(15):5659–5667.

Jung Y, Isaacs JS, Lee S, Trepel J, Liu ZG, Neckers L. Hypoxia-inducible factor induction by tumour necrosis factor in normoxic cells requires receptor-interacting protein-dependent nuclear factor kappa B activation. *Biochem J*. 2003:**370**(Pt 3): 1011–1017.

Lee M, Park JJ, Lee YS. Adhesion of ST6Gal I-mediated human colon cancer cells to fibronectin contributes to cell survival by integrin beta1-mediated paxillin and AKT activation. *Oncol Rep*. 2010:**23**(3):757–761.

Liberti MV, Locasale JW. The Warburg effect: how does it benefit cancer cells? *Trends Biochem Sci*. 2016:**41**(3):211–218.

Liu N, Zhu M, Linhai Y, Song Y, Gui X, Tan G, et al. Increasing HER2 alpha2,6 sialylation facilitates gastric cancer progression and resistance via the Akt and ERK pathways. *Oncol Rep*. 2018:**40**(5): 2997–3005.

Lu J, Gu J. Significance of beta-galactoside alpha2,6 sialyltranferase 1 in cancers. *Molecules*. 2015:**20**(5):7509–7527.

Menendez JA, Alarcon T. Metabostemness: a new cancer hallmark. *Front Oncol*. 2014:**4**:262.

Munkley J, Elliott DJ. Hallmarks of glycosylation in cancer. *Oncotarget*. 2016:**7**(23):35478–35489.

Orofiamma LA, Vural D, Antonescu CN. Control of cell metabolism by the epidermal growth factor receptor. *Biochim Biophys Acta Mol Cell Res*. 2022:**1869**(12):119359.

Park JJ, Lee M. Increasing the alpha 2, 6 sialylation of glycoproteins may contribute to metastatic spread and therapeutic resistance in colorectal cancer. *Gut Liver*. 2013:**7**(6):629–641.

Parlani M, Jorgez C, Friedl P. Plasticity of cancer invasion and energy metabolism. *Trends Cell Biol*. 2023:**33**(5):388–402.

Pasto A, Bellio C, Pilotto G, Ciminale V, Silic-Benussi M, Guzzo G, et al. Cancer stem cells from epithelial ovarian cancer patients privilege oxidative phosphorylation, and resist glucose deprivation. *Oncotarget*. 2014:**5**(12):4305–4319.

Peixoto J, Lima J. Metabolic traits of cancer stem cells. *Dis Model Mech*. 2018:**11**(8):033464.

Peyssonnaux C, Zinkernagel AS, Schuepbach RA, Rankin E, Vaulont S, Haase VH, et al. Regulation of iron homeostasis by the hypoxia-inducible transcription factors (HIFs). *J Clin Invest*. 2007:**117**(7): 1926–1932.

Qian J, Zhu CH, Tang S, Shen AJ, Ai J, Li J, et al. alpha2,6-hyposialylation of c-met abolishes cell motility of ST6Gal-I-knockdown HCT116 cells. *Acta Pharmacol Sin*. 2009:**30**(7): 1039–1045.

Rahman M, Hasan MR. Cancer metabolism and drug resistance. *Meta*. 2015:**5**(4):571–600.

Rao TC, Beggs RR, Ankenbauer KE, Hwang J, Ma VP, Salaita K, et al. ST6Gal-I-mediated sialylation of the epidermal growth factor receptor modulates cell mechanics and enhances invasion. *J Biol Chem*. 2022:**298**(4):101726.

Rinkenbaugh AL, Baldwin AS. The NF-kappaB pathway and cancer stem cells. *Cell*. 2016:**5**(2):16.

Rodrigues JG, Duarte HO, Gomes C, Balmana M, Martins AM, Hensbergen PJ, et al. Terminal alpha2,6-sialylation of epidermal growth factor receptor modulates antibody therapy response of colorectal cancer cells. *Cell Oncol*. 2021a:**44**(4):835–850.

Rodrigues JG, Duarte HO, Reis CA, Gomes J. Aberrant protein glycosylation in cancer: implications in targeted therapy. *Biochem Soc Trans*. 2021b:**49**(2):843–854.

Sancho P, Barneda D, Heeschen C. Hallmarks of cancer stem cell metabolism. *Br J Cancer*. 2016:**114**(12):1305–1312.

Schultz MJ, Holdbrooks AT, Chakraborty A, Grizzle WE, Landen CN, Buchsbaum DJ, et al. The tumor-associated glycosyltransferase ST6Gal-I regulates stem cell transcription factors and confers a cancer stem cell phenotype. *Cancer Res*. 2016:**76**(13): 3978–3988.

Schultz MJ, Swindall AF, Wright JW, Sztul ES, Landen CN, Bellis SL. ST6Gal-I sialyltransferase confers cisplatin resistance in ovarian tumor cells. *J Ovarian Res*. 2013:**6**(1):25.

Seales EC, Jurado GA, Brunson BA, Wakefield JK, Frost AR, Bellis SL. Hypersialylation of beta1 integrins, observed in colon adenocarcinoma, may contribute to cancer progression by up-regulating cell motility. *Cancer Res*. 2005:**65**:4645–4652.

Semenza GL. Targeting HIF-1 for cancer therapy. *Nat Rev Cancer*. 2003:**3**(10):721–732.

Shi R, Liao C, Zhang Q. Hypoxia-driven effects in cancer: characterization, mechanisms, and therapeutic implications. *Cell*. 2021:**10**(3):678.

Smithson M, Irwin R, Williams G, Alexander KL, Smythies LE, Nearing M, et al. Sialyltransferase ST6GAL-1 mediates resistance to chemoradiation in rectal cancer. *J Biol Chem*. 2022:**298**(3):101594.

Snyder V, Reed-Newman TC, Arnold L, Thomas SM, Anant S. Cancer stem cell metabolism and potential therapeutic targets. *Front Oncol*. 2018:**8**:203.

Swindall AF, Londoño-Joshi AI, Schultz MJ, Fineberg N, Buchsbaum DJ, Bellis SL. ST6Gal-I protein expression is upregulated in human epithelial tumors and correlates with stem cell markers in normal tissues and colon cancer cell lines. *Cancer Res*. 2013:**73**(7):2368–2378.

Tanner LB, Goglia AG, Wei MH, Sehgal T, Parsons LR, Park JO, et al. Four key steps control glycolytic flux in mammalian cells. *Cell Syst*. 2018:**7**(1):49–62 e48.

Thongon N, Zucal C, D'Agostino VG, Tebaldi T, Ravera S, Zamporlini F, et al. Cancer cell metabolic plasticity allows resistance to NAMPT inhibition but invariably induces dependence on LDHA. *Cancer Metab*. 2018:**6**(1):1.

van Uden P, Kenneth NS, Rocha S. Regulation of hypoxia-inducible factor-1alpha by NF-kappaB. *Biochem J*. 2008:**412**(3):477–484.

Warburg O. The metabolism of carcinoma cells. *Cancer Res*. 1925:**9**(1):148–163.

Warburg O, Wind F, Negelein E. The metabolism of Tumors in the body. *J Gen Physiol*. 1927:**8**(6):519–530.

Wichert B, Milde-Langosch K, Galatenko V, Schmalfeldt B, Oliveira-Ferrer L. Prognostic role of the sialyltransferase ST6GAL1 in ovarian cancer. *Glycobiology*. 2018:**28**(11):898–903.

Xiao H, Woods EC, Vukojicic P, Bertozzi CR. Precision glycocalyx editing as a strategy for cancer immunotherapy. *Proc Natl Acad Sci*. 2016:**113**(37):10304–10309.